J Neurophysiol 97: 647–658, 2007.
First published October 25, 2006; doi:10.1152/jn.00777.2006.

Cellular Mechanisms of Suppressive Interactions Between Somatosensory Responses In Vivo

Michael J. Higley and Diego Contreras
Department of Neuroscience, University of Pennsylvania, School of Medicine, Philadelphia, Pennsylvania

Submitted 27 July 2006; accepted in final form 20 October 2006

Higley MJ, Contreras D. Cellular mechanisms of suppressive interactions between somatosensory responses in vivo. *J Neurophysiol* 97: 647–658, 2007. First published October 25, 2006; doi:10.1152/jn.00777.2006. The neural integration of afferent inputs evoked by spatiotemporally distributed sensory stimuli is a critical step in the formation of coherent and continuous perceptual representations. Integration mechanisms in various systems include linear and nonlinear summation of sensory responses. One well-known example in the rat barrel system is the suppressive interaction between responses to the consecutive deflection of neighboring whiskers. The mechanism underlying cross-whisker suppression has long been postulated to rely on intracortical postsynaptic inhibition, although this hypothesis has been challenged by recent reports. Here we show, using intracellular and extracellular recordings in vivo, that cross-whisker suppression occurs in the absence of cortical activity. Instead, suppression arises from local circuit operations at multiple levels of the subcortical afferent pathway and is amplified by the nonlinear transformation of synaptic input into spike output in both the thalamus and cortex. Because these cellular processes are common to neural circuits subserving visual and auditory modalities, we propose that the suppressive mechanisms elucidated here are a general property of thalamocortical sensory systems.

INTRODUCTION

The generation of coherent perceptual experiences depends on the integration of complex sensory inputs that are discontinuously represented over multiple levels of afferent processing. This postulate is well illustrated by the rat barrel system. While exploring their environment, rats repetitively sweep their mystacial vibrissae across surfaces, resulting in a complex spatial and temporal pattern of individual whisker deflections (Carvell and Simons 1990; Hartmann et al. 2003; Sachdev et al. 2001). The neural responses to such stimuli subserve detailed perceptual analysis because rats can use their vibrissae for spatial localization, object recognition, and texture discrimination (Brecht et al. 1997; Carvell and Simons 1990; Krupa et al. 2001). Understanding how complex afferent inputs give rise to perception requires a detailed description of sensory integration at the neuronal level.

One form of sensory integration that has been well characterized is cross-whisker suppression, where deflection of a single whisker strongly reduces the neural response to a subsequent deflection of a neighboring whisker (Brumberg et al. 1996; Higley and Contreras 2005; Kida et al. 2005; Simons and Carvell 1989). Suppression magnitude is dependent on stimulus features, including interdeflection interval, direction of whisker deflection, and spatial arrangement of the paired whiskers (Brumberg et al. 1996; Higley and Contreras 2003, 2005; Kida et al. 2005; Simons and Carvell 1989). Similar forms of somatosensory suppression after paired tactile stimuli have been described for primates (Gardner and Costanzo 1980; Laskin and Spencer 1979b) as well as in human psychophysical studies (Laskin and Spencer 1979a). Functionally, suppression has been proposed to enhance both feature discrimination and neuronal sensitivity to complex naturalistic stimuli (Gardner and Costanzo 1980; Laskin and Spencer 1979a; Mountcastle 1974; Simons and Carvell 1989). Moreover, suppression also occurs in the visual (Bair 2005) and auditory (Schreiner et al. 2000) systems, suggesting that it may be a general feature of sensory integration.

Although several studies have described the phenomenon of cross-whisker suppression, the underlying cellular mechanisms remain elusive. Local inhibition mediated by cortical interneurons has been considered a likely explanation (Brumberg et al. 1996; Moore et al. 1999; Simons and Carvell 1989). However, recent studies have challenged this view, demonstrating that cortical suppression involves a reduction in both excitatory and inhibitory input (Higley and Contreras 2003, 2005). These findings suggest that suppression is inherited from earlier stages of somatosensory processing such as the thalamus or brain stem.

In the present study, we combine extracellular and intracellular recordings in the cortex, thalamus, and brain stem to demonstrate that suppression is not dependent on intracortical inhibition. Instead, it arises from a combination of reduced trigeminothalamic input, postsynaptic inhibition of thalamic neurons, and amplification by spike threshold in the thalamus and cortex. Our results show that sensory integration occurs by a synergistic interaction of local circuits at multiple stages in the afferent pathway.

METHODS

Surgery and preparation

Experiments were conducted in accordance with the ethical guidelines of the National Institutes of Health and with the approval of the Institutional Animal Care and Use Committee of the University of Pennsylvania. Adult male Sprague–Dawley rats (300–350 g, $n = 59$) were anesthetized with isoflurane (0.5–1.0%), paralyzed with gallamine triethiodide, and artificially ventilated. A craniotomy was made directly above either the barrel cortex (1.0–3.0 mm A/P, 4.0–7.0 mm M/L), the medial ventroposterior thalamic nucleus (VPm, 3.0 mm A/P, 3.0 mm M/L), or the principal trigeminal nucleus (PrV, 9.7 mm A/P, 2.8 mm M/L) and the dura was resected.

Address for reprint requests and other correspondence: D. Contreras, Department of Neuroscience, University of Pennsylvania, School of Medicine, 215 Stemmler Hall, Philadelphia, PA 19104 (E-mail: diegoc@mail.med.upenn.edu).

The costs of publication of this article were defrayed in part by the payment of page charges. The article must therefore be hereby marked "*advertisement*" in accordance with 18 U.S.C. Section 1734 solely to indicate this fact.

Electrophysiological recordings

Recordings of local field potentials (LFPs) across the cortical depth were performed with 16-channel silicon probes (University of Michigan Center for Neural Communication Technology, Ann Arbor, MI). Probe recording sites were separated by 100 μm and had impedances of 1.5–2.0 MΩ at 1 kHz. The probe was lowered into the brain under visual guidance, oriented normal to the cortical surface, until the most superficial recording site was aligned with the surface (see Fig. 1). LFP signals were amplified and filtered at 0.1 Hz to 10 kHz (FHC, Bowdoinham, ME). Extracellular unit recordings were obtained using glass-insulated tungsten electrodes with an impedance of 1.5 MΩ at 1 kHz (Alpha-Omega, Alpharetta, GA). Signals were amplified and filtered at 500 Hz to 10 kHz (FHC). Intracellular recordings from VPm were performed with glass micropipettes pulled on a P-97 Brown Flaming puller (Sutter Instrument Company, Novato, CA). Pipettes were filled with 3 M potassium acetate and had DC resistances of 60–80 MΩ. A high-impedance amplifier (low-pass filter of 5 kHz) with active bridge circuitry (Cygnus Technology, Delaware Water Gap, PA) was used to record and inject current into cells. All recordings were digitized at 20 kHz using Spike2 (C.E.D., Cambridge, UK). The electroencephalogram was recorded from a screw placed in the skull over the contralateral parietal cortex.

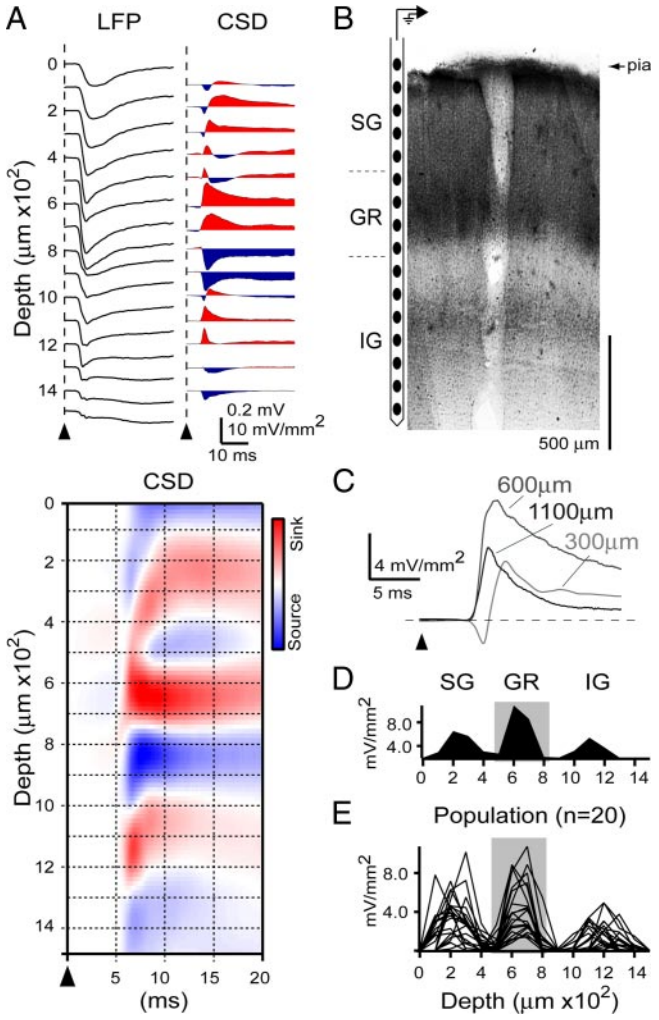

FIG. 1. Current source density (CSD) analysis of the cortical response to whisker deflection. *A*, *left column of traces*: local field potentials (LFPs) evoked by principal whisker (PW) deflection (filled triangle). *Right column*: CSD illustrates corresponding current sinks (red) and sources (blue). Cortical depth is indicated at *left*. Color image at bottom illustrates the CSD data, linearly interpolated across depth, for the first 20 ms of the response. *B*: track created by 16-channel probe (depicted in schema at *left*), recovered in coronal sections of barrel cortex stained for cytochrome oxidase. Granular layer 4 (GR) is shown by darkly stained barrels. Range of depths corresponding to GR, supragranular (SG), and infragranular (IG) depths is indicated. *C*: single traces of PW-evoked (filled triangle) CSD responses from *A*, recorded at the depths indicated. Upward deflections reflect current sinks. *D*: CSD profile of the PW-evoked response in *A*. Value on *y*-axis is the integral of the positive half-wave–rectified CSD trace over the first 20-ms postdeflection for each recording depth given on the *x*-axis. Values are derived from the raw CSD traces. *E*: CSD profiles as in *D* for the population ($n = 20$).

Whisker stimulation

For each recording, the principal whisker (PW) and the immediately caudal adjacent whisker (AW) were mechanically deflected in the caudal direction (200 μm) by applying a square voltage pulse to a piezoelectric stimulator (Piezo Systems, Cambridge, MA). For PrV recordings, we characterized the effect of prior deflection of the four surrounding AWs (caudal, dorsal, rostral, and ventral).

Cortical inactivation

To inactivate cortical activity, a dental acrylic well was built around the craniotomy and filled with buffered normal saline to obtain baseline recordings. Control saline was then replaced with a solution of 2.5 mM muscimol (Sigma Chemical) in buffered saline, which was allowed to diffuse passively into the cortex. Cortical LFPs and single units in layers 4 and 6 were monitored continuously to confirm elimination of spontaneous cortical activity across all cortical depths (see Fig. 3). In a separate series of experiments, we recorded single units in cortical layers 4 and 6 to confirm elimination of spontaneous and evoked activity across all cortical depths (Fig. 3), which was usually complete within 45 min of muscimol application.

Data analysis

LFPs from the 16-channel probes were used to calculate the current source density (CSD) of the cortical whisker-evoked responses according to the methods of Swadlow et al. (2002). We chose to carry out detailed analyses on the CSD values because of the inherent lack of spatial resolution across cortical depths provided by monopolar LFP recordings.

Briefly, the one-dimensional CSD was derived from the second spatial derivative of the LFP data as described by Freeman and Nicholson (1975)

$$(\partial^2\Phi/\partial z^2) = [\Phi(z + 2\Delta z) - 2\Phi(z) + \Phi(z - 2\Delta z)]/(2\Delta z)^2$$

where Φ is the LFP, z is the vertical coordinate depth of the probe, and Δz is the interrecording site distance (100 μm in the present study). Upper and lower boundaries for CSD calculation were obtained by extrapolating recordings from the first and last recording sites. To facilitate visualization of the CSD data, we produced color image plots by linearly interpolating the recordings along the vertical axis as in a previous study (Swadlow et al. 2002). However, all quantifications of CSD data were made using the raw data. To quantify the amplitude and spatial distribution of current sinks, thought to directly reflect synaptic excitation (Mitzdorf 1985), we generated a laminar CSD profile for the evoked response by integrating the half-wave–rectified raw CSD trace (thus including only current sinks) over the first 20 ms of the response for each recording site. For suppression analysis, we summed the values from the CSD profile for supragranular (SG, 0–500 μm), granular (GR, 500–800 μm), and infragranular (IG, 800–1,500 μm) depths.

Single units in cortex, VPm, and PrV with constant amplitude, spike shape, and signal to noise ratios of $\geq$4:1 were extracted with a simple threshold algorithm. Multiunit recordings in VPm consisted of two to four units of varying amplitude that could not be reliably

separated. Peristimulus time histograms (PSTHs) were constructed for unit data using bins of either 1 ms (VPm) or 0.2 ms (PrV).

RESULTS

We recorded the vertical distribution of local cortical field potentials and currents evoked by whisker deflection in 20 isoflurane-anesthetized rats. Figure 1*A* illustrates the average LFPs and derived CSD traces after PW deflection (filled triangle) for a representative experiment. The most superficial recording site was aligned with the pial surface under microscopic guidance. The depth below the cortical surface of each recording site is given on the left axis (intersite distance of 100 μm). Depths of 500–800 μm correspond to granular (GR) layer 4, with more superficial and deeper depths corresponding to supragranular (SG) and infragranular (IG) layers, respectively. Figure 1*B* illustrates an example of the recovered probe track in a coronal section of barrel cortex stained for cytochrome oxidase. The GR layer is evident from the darkly stained barrels.

The PW-evoked LFP consisted of a depth-negative wave that reached peak magnitude in the middle cortical depths at a latency of 8.5 ms. CSD analysis revealed that PW deflection evoked a large current sink (red, positive-going area) within the GR layer and smaller sinks in SG and IG layers. Distribution of current sinks and sources over the first 20 ms of the response is illustrated in greater detail by the expanded depth-interpolated color image (Fig. 1*A*, *bottom*) and the individual CSD traces (Fig. 1*C*) from recording sites at depths of 300, 600, and 1,100 μm (light gray, medium gray, and dark gray, respectively). PW-evoked current sinks began earliest in GR and IG layers with a latency of 4.6 ms. A current sink then rapidly evolved in SG layers after a delay of 2 ms. Figure 1*D* illustrates the CSD profile (see METHODS) for the example in Fig. 1*A*, which closely captures the magnitude and spatial distribution of evoked current sinks seen in the color image plot (gray box highlights GR layer). Figure 1*E* illustrates the CSD profiles of the PW-evoked responses for all 20 experiments included in the present study. Although amplitudes varied across experiments, PW deflection uniformly resulted in spatially segregated current sinks located in SG, GR, and IG depths, similar to those found in previous studies using both CSD analysis (Di et al. 1990; Swadlow et al. 2002) and voltage-sensitive dye imaging in vitro (Laaris et al. 2000; Llinás et al. 2002).

CSD analysis of cross-whisker suppression

To study cross-whisker suppression, we calculated the whisker-evoked cortical CSD after deflection of the PW alone or preceded 20 ms by the deflection of the caudal AW. Figure 2, *A* and *B* illustrates the results for an example experiment. PW deflection (Fig. 2*A*, *first panel*, filled triangle) evoked a spatially segregated pattern of current sinks that appeared earliest in middle and deep layers (5.2 ms) and then spread superficially. Individual CSD traces from 300, 700, and 1,400 μm depth are shown at the *far right* (PW, dark gray), and the CSD profile for the initial 20 ms of the PW-evoked response is shown in Fig. 2*B* (*left*). AW deflection (Fig. 2*A*, *second panel*, open triangle) evoked a similar spatiotemporal pattern of sinks and sources, although smaller in magnitude.

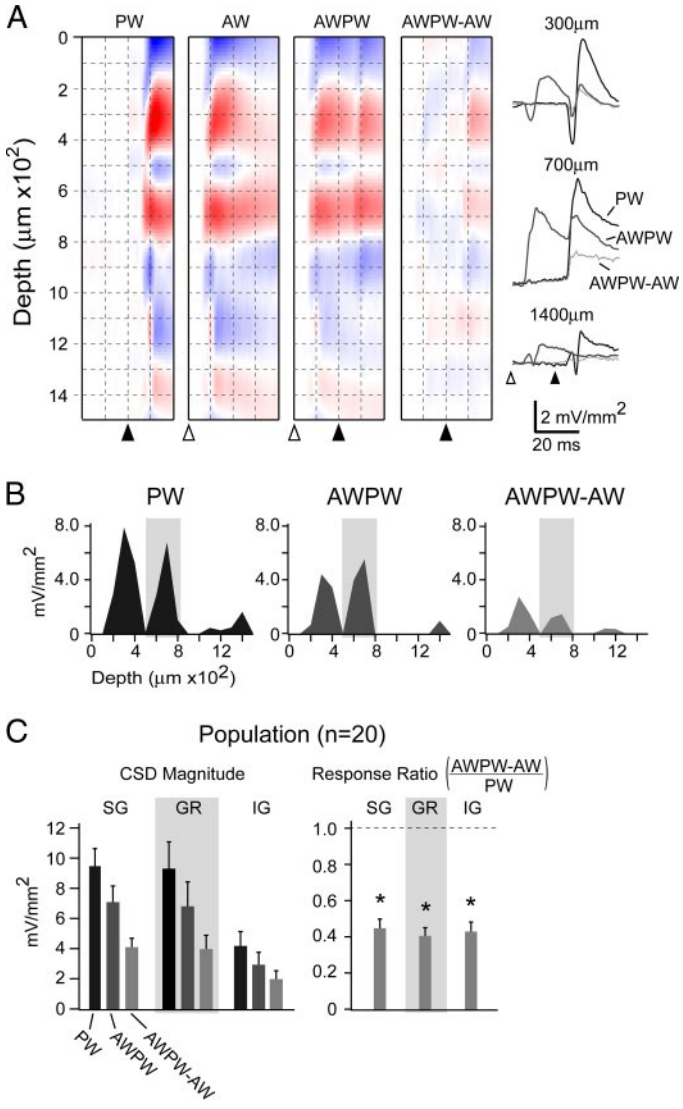

FIG. 2. Suppression of whisker-evoked CSD responses. *A*: CSD images, corresponding to PW deflection alone (filled triangle), adjacent whisker (AW) deflection alone (open triangle), paired deflection of AW preceding PW by 20 ms (AWPW), and paired response after subtracting the response to AW deflection alone (AWPW − AW). Current sinks and sources are shown in red and blue, respectively. Cortical depth is indicated on the vertical axis. Single traces of CSD responses are shown at the *right* for the depths indicated. Responses are for PW deflection (dark gray), paired deflection (AWPW, medium gray), and paired deflection after subtracting the response to AW deflection alone (AWPW − AW, light gray). *B*: CSD profiles from the experiment in *A* for PW (*left*, dark gray), AWPW (*center*, medium gray), and AWPW − AW (*right*, light gray) responses. *C*, *left graph*: population data (means ± SE, $n = 20$) for PW (dark gray), AWPW (medium gray), and AWPW − AW (light gray) CSD response magnitudes, calculated by summing values from CSD profiles over depths corresponding to SG (0–500 μm), GR (500–800 μm), and IG (800–1,500 μm) layers. Gray box highlights GR layer values. *Right graph*: population response ratios (AWPW − AW)/(PW) for each depth. All response ratios were significantly <1, indicating suppression.

When AW deflection preceded PW deflection by 20 ms (Fig. 2*A*, *third panel*), the resulting PW-evoked current sinks were reduced in total magnitude, despite overlapping the AW-evoked response. This suppression is evident in the individual CSD traces to the *right* (AWPW, medium gray) and the CSD profile (Fig. 2*B*, *center*). Because of the temporal overlap of the responses, we also plotted the CSD image after subtracting the

contribution arising from AW deflection alone (Fig. 2*A*, *fourth panel*). This result, clearly seen in the individual CSD traces to the *right* (AWPW − AW, light gray) and the CSD profile below (Fig. 2*B*, *right*), indicates that the main effect of the preceding AW deflection was a strong reduction in PW-evoked response magnitude across all depths.

To quantify the data, we summed response magnitudes from the CSD profiles for SG (0–500 μm), GR (500–800 μm), and IG (800–1,500 μm) layers. For the experiment in Fig. 2, the PW-evoked response magnitude was 16.5, 10.8, and 3.0 mV/mm^2 for SG, GR, and IG layers, respectively. The PW-evoked response after AW deflection was 8.6, 10.5, and 1.9 mV/mm^2. After subtracting the contribution of the AW-evoked response, these values were reduced to 4.8, 2.7, and 1.2 mV/mm^2.

We also calculated these values for the population of experiments ($n = 20$). The mean PW-evoked response magnitude was 9.5 ± 1.1, 9.3 ± 1.3, and 4.1 ± 0.6 mV/mm^2 for SG, GR, and IG layers, respectively (Fig. 2*C*, *left*, dark gray bars). The mean AW-evoked response magnitude was 8.2 ± 1.3, 8.3 ± 1.5, and 3.5 ± 0.7 mV/mm^2 (data not shown). The mean PW-evoked responses after AW deflection were 7.1 ± 1.2, 6.7 ± 1.3, and 3.1 ± 0.6 mV/mm^2 (Fig. 2*C*, *left*, medium gray bars). These values were reduced to 4.1 ± 0.7, 4.0 ± 0.8, and 1.9 ± 0.4 mV/mm^2 after subtracting the contribution of the preceding AW-evoked response (Fig. 2*C*, *left*, light gray bars).

We quantified suppression by calculating a response ratio (RR), expressed as the magnitude of the PW-evoked response when preceded by AW deflection (after subtracting the contribution of the AW-evoked response) divided by the response magnitude to PW deflection alone: RR = (AWPW − AW)/(PW). Preceding AW deflection resulted in mean RRs for the population that were significantly <1.0 for SG (0.45 ± 0.05, Student's *t*-test, $P < 0.001$), GR (0.40 ± 0.04, $P < 0.001$), and IG (0.43 ± 0.04, $P < 0.001$) layers (Fig. 2*C*, *right*). There were no significant differences in RRs across the three laminar groups (repeated-measures ANOVA, $P = 0.4$). In summary, preceding AW deflection strongly and uniformly suppressed the local cortical current sinks evoked by subsequent PW deflection.

Cross-whisker suppression is maintained after cortical inactivation

To determine whether intracortical mechanisms are necessary for suppression of PW-evoked responses, we characterized whisker-evoked response integration after pharmacologically inactivating the cortex using the γ-aminobutyric acid type A ($GABA_A$) agonist muscimol. Figure 3*A* (*left column*, CTL) illustrates spontaneous LFPs for six different recording depths as well as the contralateral surface EEG under control conditions. All channels exhibited synchronized oscillations typical of light to moderate levels of isoflurane anesthesia. After application of 2.5 mM muscimol to the brain surface (see METHODS), spontaneous cortical activity gradually diminished in amplitude, with superficial layers inactivating earliest (Fig. 3*A*, *columns 2*, *3*, and *4* show cortical activity 5, 15, and 45 min after muscimol application, respectively). By 45 min postmuscimol application, all cortical layers were silent. However, activity in the contralateral hemisphere was intact, although reduced in amplitude, likely reflecting the withdrawal of callosal inputs. To confirm that sensory stimulation did not activate cortical circuits after muscimol application, we recorded LFPs and single-unit responses to PW deflection from depths corresponding to layer 4. Figure 3*B* illustrates an example recording (770 μm depth) where the LFP ($L4_{LFP}$, top 10 superimposed traces) and unit ($L4_{unit}$, bottom 10 superimposed traces and corresponding PSTHs) responses were re-

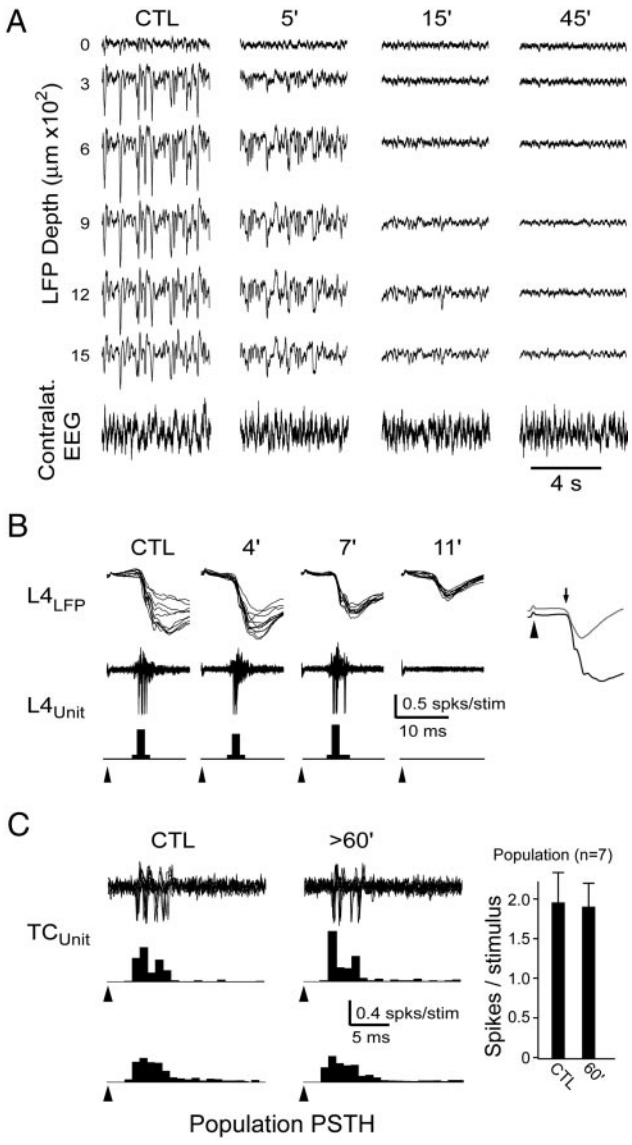

FIG. 3. Pharmacological inactivation of cortical activity. *A*, *left column*: simultaneously recorded spontaneous LFPs at 6 cortical depths (indicated at *left*). *Bottom trace*: surface electroencephalogram (EEG) from the contralateral hemisphere. Additional columns are for the same recording sites taken after surface application of 2.5 mM muscimol at the times indicated at *top*. *B*, *left column*: 10 overlaid traces of a PW-evoked (filled triangle) LFP and a single-unit response recorded from the same electrode in layer 4 (L4) under control conditions. *Bottom histogram* (bin size = 1 ms): cumulative spike output for 40 deflections. Additional columns illustrate same recordings made after muscimol application at the times indicated at *top*. *Inset*: average LFP before (dark gray) and after (light gray) cortical inactivation. Remaining response reflects direct thalamocortical inputs. Note that LFP onset latency (arrow) is unchanged. *C*: 10 overlaid traces of a PW-evoked single unit response in VPm before and after cortical inactivation. *Top histograms* (bin size = 1 ms): cumulative spike output from this unit for 40 deflections. *Bottom histograms* and graph at the *right* show the population responses of all VPm units tested before and after cortical inactivation ($n = 7$, no significant difference).

corded simultaneously from the same electrode. PW deflection before muscimol application (CTL) evoked a large LFP and spike response of the unit (0.7 spike/stimulus). However, after 11 min of muscimol application, the LFP was strongly reduced in magnitude and neuronal firing was eliminated. Inspection of the average LFPs (Fig. 3*B*, *inset*) revealed that the remaining evoked potential (light gray) had an onset latency similar to that of the control evoked potential (dark gray, small arrow indicates onset), suggesting that the LFP after muscimol reflected direct postsynaptic excitation by thalamic inputs without subsequent engagement of cortical circuits. Similar abolition of layer 4 unit responses and reduction of LFPs was observed in five additional experiments. Muscimol also eliminated spontaneous and whisker-evoked suprathreshold activity in unit recordings from deep infragranular layers (1,400–1,600 μm depth, $n = 5$, data not shown), indicating that the muscimol penetrated the entire cortical depth.

We also recorded a number of single units in VPm ($n = 7$) to determine whether cortical inactivation altered the thalamic response to whisker deflection. Figure 3*C* illustrates one example where the control thalamic response (1.7 spikes/stimulus) was minimally affected 60 min after muscimol application (1.9 spikes/stimulus) despite total cortical inactivation (not shown). This result was confirmed for the population of thalamic units tested with cortical inactivation because the mean response magnitudes for control and muscimol conditions were 2.0 ± 0.4 and 1.9 ± 0.3 spikes/stimulus, respectively (paired *t*-test, $P = 0.3$). In sum, these data show that muscimol application successfully inactivated all cortical activity while preserving subcortical responses.

We next characterized whisker-evoked response integration after cortical inactivation. Figure 4, *A* and *B* illustrates data from the same experiment shown in Fig. 2 after cortical inactivation. PW deflection (Fig. 4*A*, *first panel*, filled triangle) evoked an early current sink simultaneously in GR and IG layers at similar onset latency as under control conditions, although both response magnitude (3.0 and 0.6 mV/mm^2 for GR and IG layers, respectively) and duration were decreased (note change in magnitude scale from Fig. 2*A*). No current sink was evoked in SG layers. The spatial correspondence of the cortical response with regions of thalamocortical terminal arborizations (Arnold et al. 2001; Jensen and Killackey 1987) suggests that the CSD data directly reflect thalamocortical synaptic inputs. This finding is also seen in the individual CSD traces at the *far right* (PW, dark gray) and the CSD profile (Fig. 4*B*, *left*). AW deflection (Fig. 4*A*, *second panel*, open triangle) evoked a smaller but clearly present cortical response consisting of GR and IG current sinks.

When AW deflection preceded PW deflection by 20 ms (Fig. 4*A*, *third panel*), the resulting PW-evoked current sinks were reduced in magnitude (1.2 and 0.3 mV/mm^2 for GR and IG layers, respectively). The suppression is also evident in the individual CSD traces to the *right* (AWPW, medium gray) and in the CSD profile below (Fig. 4*B*, *center*). We again subtracted the contribution from the AW-evoked response (Fig. 4*A*, *fourth panel*). A reduction in response magnitude across all depths (0.7 and 0.3 mV/mm^2 for GR and IG layers, respectively) was seen in both the individual CSD traces (AWPW − AW, light gray) and the CSD profile (Fig. 4*B*, *right*).

For the population ($n = 20$), the mean PW-evoked response magnitudes in GR and IG layers (SG responses were absent in all cases) were 2.7 ± 0.5 and 1.7 ± 0.3 mV/mm^2 (Fig. 4*C*, *left*, dark gray bars). The mean AW-evoked responses were 1.9 ± 0.6 and 1.1 ± 0.3 mV/mm^2 (data not shown). The mean PW-evoked responses after AW deflection were 1.2 ± 0.2 and 1.1 ± 0.2 mV/mm^2 (Fig. 4*C*, *left*, medium gray bars). These values were reduced to 0.9 ± 0.1 and 0.9 ± 0.1 mV/mm^2 after

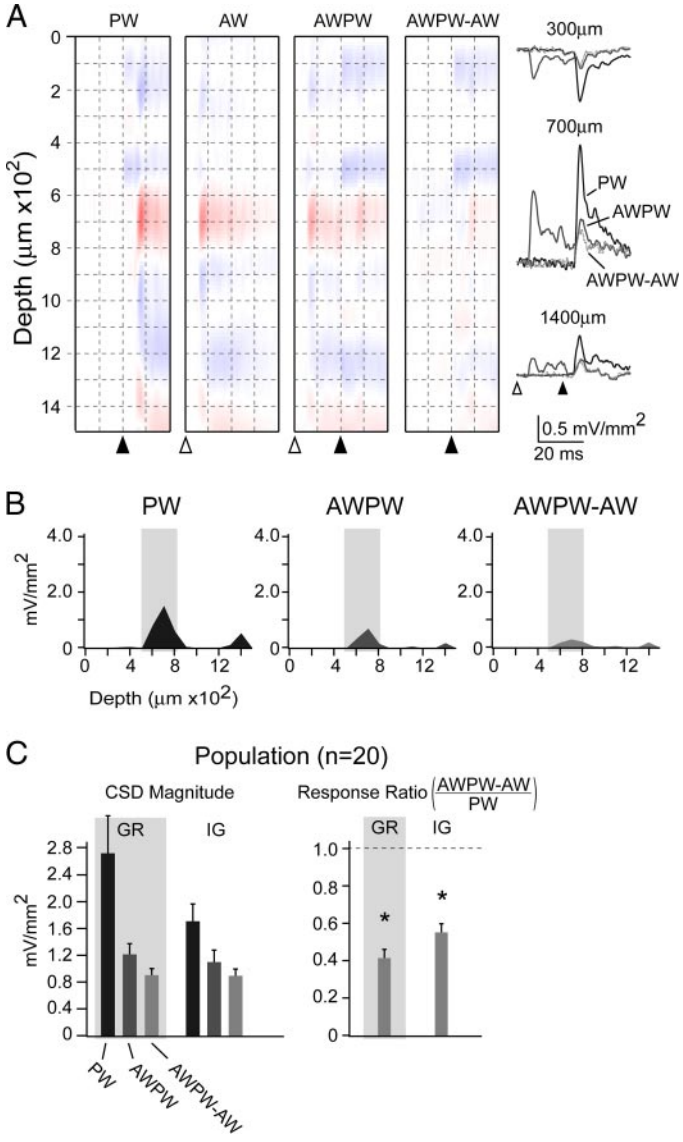

FIG. 4. Suppression of whisker-evoked CSD responses after cortical inactivation. *A*: CSD images, corresponding to PW deflection alone (filled triangle), AW deflection alone (open triangle), paired deflection of AW preceding PW by 20 ms (AWPW), and paired response after subtracting the response to AW deflection alone (AWPW − AW) for the same experiment in Fig. 1*A*. Current sinks and sources are shown in red and blue, respectively. Cortical depth is shown on the vertical axis. Single traces of CSD responses are shown at the *right* for the depths indicated. Responses are for PW deflection (dark gray), paired deflection (AWPW, medium gray), and paired deflection after subtracting the response to AW deflection alone (AWPW − AW, light gray). *B*: CSD profiles from the experiment in *A* for PW (*left*, dark gray), AWPW (*center*, medium gray), and AWPW − AW (*right*, light gray) responses. *C*, *left graph*: population data (means ± SE, $n = 20$) for PW (dark gray), AWPW (medium gray), and AWPW − AW (light gray) CSD response magnitudes, calculated by summing values from CSD profiles over depths corresponding to GR (400–800 μm) and IG (800–1,500 μm) layers. Gray box highlights GR layer values. *Right graph*: population response ratios (AWPW − AW)/(PW) for each depth. All response ratios were significantly <1, indicating suppression.

subtracting the contribution of the AW-evoked response (Fig. 4*C*, *left*, light gray bars). The preceding AW deflection resulted in mean RRs for the population that were significantly <1.0 for both GR (0.41 ± 0.04, $P < 0.001$) and IG (0.55 ± 0.05, $P < 0.001$) layers (Fig. 4*C*, *right*). There were no significant differences between layers (paired *t*-test, $P = 0.09$). More important, the RRs after muscimol did not differ significantly from the response ratios under control conditions (paired *t*-test, $P = 0.9$ and $P = 0.1$ for GR and IG layers, respectively).

Cross-whisker suppression of thalamic output

To determine whether reduction of thalamic output could account for cortical suppression, we made extracellular recordings in VPm, the principal source of ascending sensory input to the barrel cortex. For the example single unit in Fig. 5*A*, PW deflection evoked 2.1 spikes/stimulus, whereas AW deflection evoked a smaller response of 1.4 spikes/stimulus. Preceding AW deflection reduced the PW-evoked response to 0.2 spike/stimulus. To quantify this reduction, we calculated the RR expressed as the magnitude of the PW-evoked response after AW deflection divided by the magnitude of the response to PW deflection alone. Because the duration of the AW-evoked responses was rarely >20 ms, we did not systematically subtract an AW-evoked contribution from the response to paired deflection. For the unit in Fig. 5*A*, the RR was 0.11. We made similar recordings for 11 single units and 24 multiunits in VPm. The mean PW-evoked responses were 1.9 ± 0.25 and 2.6 ± 0.4 spikes/stimulus, and the mean AW-evoked responses were 1.4 ± 0.3 and 2.5 ± 0.4 spikes/stimulus for single and multiunits, respectively (Fig. 5*B*, *left*). After AW deflection, the mean PW responses were reduced to 0.7 ± 0.2 and 1.3 ± 0.3 spikes/stimulus (Fig. 5*B*, *left*), corresponding to average RRs that were significantly <1.0 for both single units (0.37 ± 0.08, $P < 0.001$) and multiunits (0.4 ± 0.06, $P < 0.001$, Fig. 5*B*, *right*).

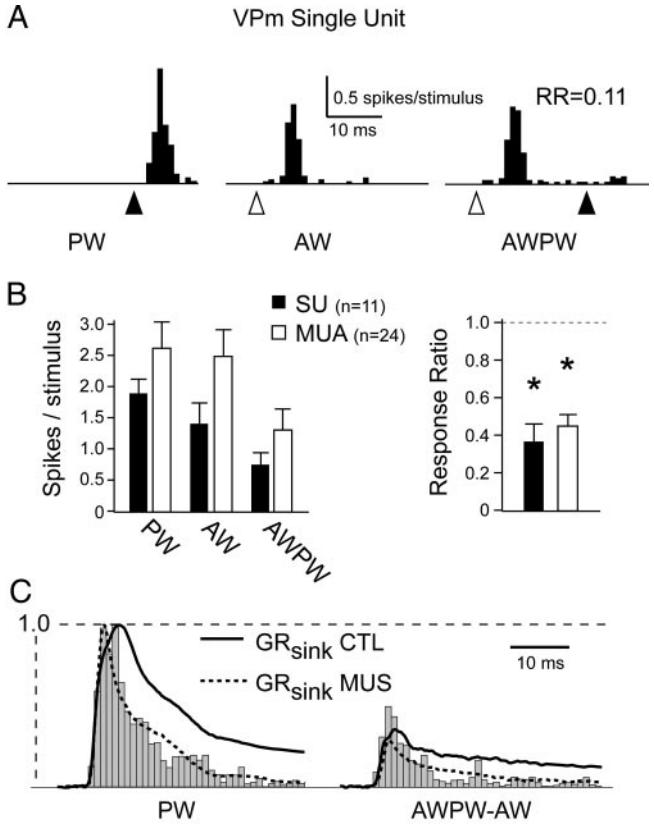

FIG. 5. Suppression of whisker-evoked responses in VPm. *A*: responses of an example single unit in VPm to PW deflection (filled triangle, *left*), AW deflection (open triangle, *center*), and paired AWPW deflection (*right*). Histograms (bin size = 1 ms) are the cumulative spike output to 40 deflections. *B*, *left graph*: average values for spike output after PW, AW, and paired AWPW deflections for the populations of single units (filled bars, $n = 11$) and multiunits (open bars, $n = 24$). *Right graph*: average response ratios for single and multiunits. Both values are significantly <1, indicating suppression. *C*, *left*: for PW deflection, the population histogram of thalamic spike output overlaid by the average GR layer current sinks before (solid line, Gr_{sink}CTL) and after (dashed line, Gr_{sink}MUS) muscimol application. Traces and histograms were normalized to a peak magnitude of 1.0 to facilitate comparison. *Right*: same traces and histogram for the paired AWPW deflection (after subtracting the response to AW deflection alone for the current sinks). Traces and histograms were scaled to the same value as their correspondents at the *left*.

The close agreement between the thalamic and cortical response ratios suggests that the cortically observed suppression could be explained by a reduction in thalamocortical input. If so, the observed PW-evoked current sinks in the GR input layer after cortical inactivation should closely follow the time course of the evoked thalamic population response. Therefore in Fig. 5*C* (*left*), we compared the population histogram of thalamic units with the average GR layer current sinks calculated before (solid line) and after (dashed line) cortical inactivation for PW deflection alone. To compare the relative timing of the three responses, each was normalized to a peak amplitude of 1 and the response onsets were horizontally aligned. Before adjusting the traces, the delay between the initial thalamic population response and the earliest detectable cortical response was 2 ms. Figure 5*C* (*right*) illustrates the same comparison for the paired AWPW deflection after subtracting the preceding AW-mediated contribution to the cortical responses. The peak amplitudes were scaled by the same factor as on the *left* to illustrate the proportional reduction in response magnitude caused by preceding AW deflection.

For both the PW and paired deflections, the time course of the GR layer current sinks after muscimol application closely followed that of the thalamic output, suggesting that the cortical response was generated entirely by thalamocortical synaptic inputs and that cortical suppression, after inactivation, can be entirely accounted for by the reduction in thalamic spikes. However, when the cortex was active, the duration of the cortical response was increased, suggesting that, under normal conditions, corticocortical activity contributes to the observed whisker responses. Nevertheless, the magnitude of suppression remained unchanged, further supporting the conclusion that reduced thalamic output can account for cortical suppression.

Cross-whisker suppression in PrV

To test whether the observed reduction in thalamic responses is inherited from suppression in the brain stem, we recorded single units in PrV ($n = 24$), the principal source of ascending whisker input to VPm. We quantified the effect of deflection of each of the four surrounding AWs on PW response magnitude. The example unit in Fig. 6*A* responded to deflection of the PW (3.2 spikes/stimulus) as well as three AWs (2.9, 0.9, and 1.0

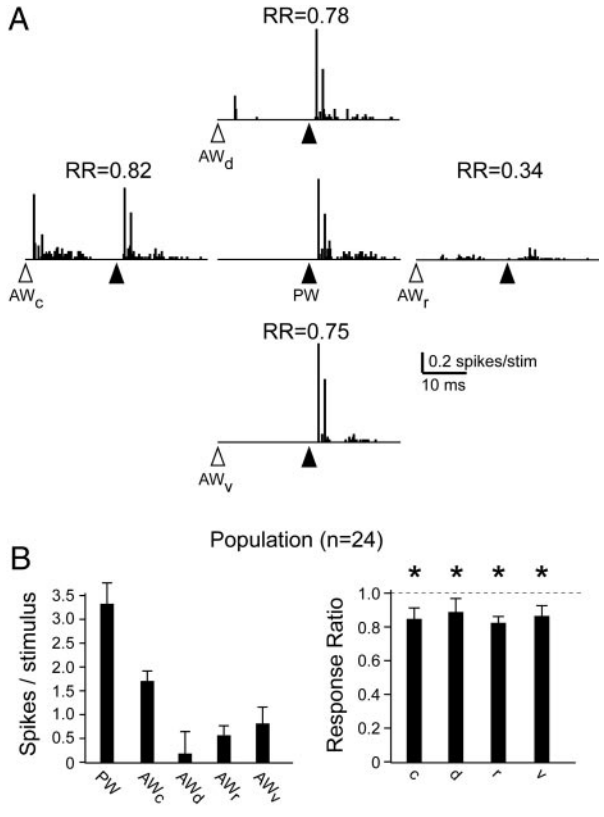

FIG. 6. Suppression of whisker-evoked responses in PrV. *A*: responses of an example single unit in PrV to PW deflection alone (filled triangle, *center*) and paired deflection of the PW preceded by each of the 4 surrounding AWs (open triangles, *left*, *top*, *right*, and *bottom*). Histograms (bin size = 0.2 ms) are the cumulative spike output to 40 deflections. *B*, *left graph*: average values for spike output after deflection of the PW and each of the 4 surrounding AWs (caudal, dorsal, rostral, and ventral) for the population ($n = 24$). *Right graph*: average response ratios for paired deflections of the PW with each of the surrounding AWs. All values were significantly <1, indicating suppression.

spikes/stimulus for caudal, dorsal, and rostral AWs, respectively). When AW deflection preceded PW deflection by 20 ms, the PW-evoked response was reduced for all AW positions (2.7, 2.5, 0.8, and 2.4 spikes/stimulus, yielding RRs of 0.8, 0.7, 0.3, and 0.7 for caudal, dorsal, rostral, and ventral AWs, respectively). Interestingly, for this case, the strongest suppression was mediated by deflection of an AW that evoked a particularly weak response. Nevertheless, for the population, suppression was weakly correlated with the magnitude of the AW response (Pearson's correlation, $r^2 = 0.3$, $P < 0.005$, data not shown), suggesting that the strength of suppression in PrV is related to the AW response magnitude.

For the population, PW deflection evoked 3.3 ± 0.4 spikes/stimulus, whereas AW deflection evoked a smaller response (1.7 ± 0.2, 0.2 ± 0.4, 0.6 ± 0.2, and 0.8 ± 0.3 spikes/stimulus for caudal, dorsal, rostral, and ventral AWs, respectively; Fig. 6*B*, *left*). After AW deflection, the PW-evoked response was reduced to 2.7 ± 0.2, 2.9 ± 0.4, 2.7 ± 0.4, and 2.8 ± 0.3 spikes/stimulus, yielding average RRs of 0.83 ± 0.07, 0.89 ± 0.08, 0.82 ± 0.05, and 0.87 ± 0.06 for caudal, dorsal, rostral, and ventral AWs, respectively (Fig. 6*B*, *right*). All RRs were significantly <1.0 ($P < 0.001$) but did not significantly differ across AWs (one-way ANOVA, $P = 0.9$). In summary, the data indicate that cross-whisker suppression is present in the brain stem, although of a magnitude considerably less than that in the thalamus.

Synaptic mechanisms of thalamic suppression

The extracellular data alone do not provide insight into the mechanism underlying transformation from weak suppression of spike output in the brain stem to much stronger suppression of thalamic output. Therefore we made intracellular recordings in VPm ($n = 15$) to better understand how synaptic input is coupled to spike generation in the thalamus. For the example in Fig. 7*A*, responses to PW deflection at resting V_m (−68 mV) consisted of a short-latency (3.8-ms) burst of three to four clearly distinguishable postsynaptic potentials (PSPs) that exhibited temporal summation and frequently resulted in spike generation (0.6 spike/stimulus). These presumed trigeminothalamic PSPs appeared to be unitary all-or-none events, evoked with great precision and reliability over several deflections. The synaptic events were followed by a hyperpolarization of the V_m that peaked at a latency of 40 ms and lasted 50–100 ms. The magnitude of the delayed hyperpolarization was enhanced at a depolarized V_m (−60 mV) and appeared to be completely reversed at a hyperpolarized V_m (−80 mV), consistent with $GABA_A$-mediated inhibition from the thalamic reticular nucleus (Lee et al. 1994b; Varga et al. 2002). Additionally, at the hyperpolarized V_m, the individual PSPs were subthreshold for action potential generation, although a low-threshold spike (Fig. 7*A*, curved arrow) was frequently evoked after temporal integration of multiple events. AW deflection (Fig. 7*A*, *center column*, open triangle) evoked a similar pattern of excitation followed by inhibition, although there were fewer PSPs and reduced spike output from resting V_m (0.2 spike/stimulus).

When preceded by AW deflection, PW-evoked spike output was completely eliminated (Fig. 7*A*, *right column*). This result appeared to be attributable to two distinct mechanisms: a reduction in the mean number of PW-evoked PSPs and a decrease in the amplitude of individual PSPs. Prior AW deflection reduced the mean number of PSPs occurring in the first 20 ms of the PW-evoked response from 4.5 to 3.5 PSPs/stimulus (shown for resting and hyperpolarized V_m levels; arrows indicate that PSPs occurred with constant latency over several deflections; Fig. 5*B*). The mean amplitude of the first PSP in each response was reduced from 5.4 to 3.2 mV. These values correspond to RRs for PSP number and first PSP amplitude of 0.78 and 0.59, respectively.

To assess the contribution of synaptic shunting inhibition evoked by the preceding AW deflection in reducing the amplitude of subsequent PW-evoked PSPs, we plotted V_m against the current injected through the recording pipette (Fig. 7*C*) for two time points: baseline (filled circles) and 25 ms after AW deflection (open squares), corresponding to the onset time of the PW-evoked PSP for the paired deflection. The slope of the best fit line through each set of points gives the apparent input resistance (R_{in}) of the cell at that time. For this cell, baseline R_{in} was 15.8 MΩ and decreased to 11.0 MΩ 25 ms after AW deflection, yielding RR = 0.70 for R_{in}, similar to the reduction in PW-evoked PSP amplitude.

For the population ($n = 15$), preceding AW deflection resulted in mean RRs that were significantly <1 for PSP number (0.71 ± 0.07, $P < 0.005$), PSP amplitude (0.74 ± 0.07, $P < 0.001$), and spike output (0.46 ± 0.09, $P < 0.001$,

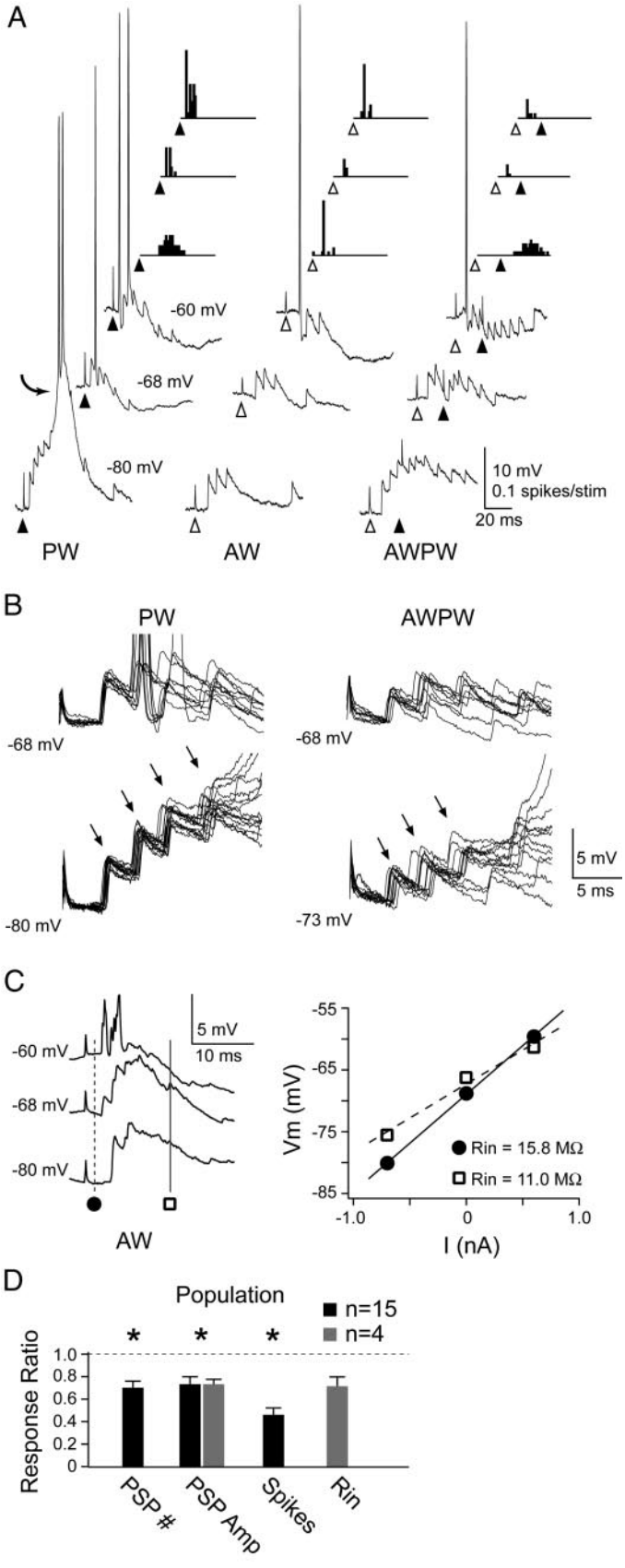

Fig. 7*D*, black bars). This value of spike suppression is similar to that seen for our extracellular single-unit recordings. The finding that spike suppression was enhanced relative to that of the underlying PSP appeared to be a result of the nonlinearity of spike threshold because small decreases in PSP amplitude resulted in strong reduction in spike output. In the subset of cells for which we calculated changes in R_{in} ($n = 4$), the mean RRs for PSP amplitude and R_{in} were 0.75 ± 0.04 and 0.72 ± 0.09, respectively (Fig. 7*D*, light gray bars), suggesting that the AW-evoked inhibition largely explains the amplitude reduction. Thus the combination of these two mechanisms can explain the increased suppression of thalamic versus trigeminal spike output.

PSP amplitude reduction might also be explained by trigeminothalamic synaptic depression arising from AW- and PW-evoked evoked spikes in the same presynaptic PrV cells. However, evidence against synaptic depression is shown in Fig. 8, where the responses to PW deflection alone and preceded by AW deflection are illustrated for another cell. Preceding AW deflection strongly suppressed spike output from 1.7 to 0.7 spikes/stimulus and also caused a reduction in PSP number (from 2.2 to 1.1 PSPs/stimulus) and amplitude (from 5.1 to 4.1 mV). These changes are illustrated by the five superimposed traces (*bottom panels*). However, AW deflection alone resulted in no discernible excitatory response, arguing against synaptic depression.

DISCUSSION

The goal of the present study was to elucidate the cellular mechanisms underlying cross-whisker suppression in the rat barrel system. Here we demonstrate that sensory suppression arises from a combination of local circuit interactions at multiple levels of processing along the afferent pathway. Modest cross-whisker suppression (roughly 15% reduction in PW-evoked spike output) occurs at the level of the brain stem, also observed as a similar reduction in the number of PW-evoked trigeminothalamic PSPs. Intrathalamic postsynaptic inhibition also appeared to decrease the amplitude of trigeminothalamic PSPs. This combined suppression of synaptic inputs was enhanced by the nonlinearity of spike threshold to yield a roughly 55% decrease in thalamic spike output, likely accounting for

FIG. 7. Suppression of whisker-evoked synaptic responses in VPm. *A*: example intracellular recording of a neuron in VPm. *Left column*: example responses to PW deflection (filled triangle) from 3 different V_m levels. Synaptic responses consisted of an initial burst of unitary postsynaptic potentials (PSPs) followed by inhibition that was hyperpolarizing from resting V_m (−68 mV). PW deflection evoked a low-threshold spike (LTS, curved arrow) from the hyperpolarized V_m level. Histograms (bin size = 1 ms) show the cumulative spike output for the corresponding V_m levels. *Center and right columns*: similar traces and histograms for responses to AW deflection (open triangle) and paired AWPW deflection. *B*: 20 overlaid traces, taken from the cell in *A* in response to PW deflection alone (*left*) or paired AWPW deflection (*right*) at both resting and hyperpolarized V_m levels, are shown. Arrows indicate reliable fixed-latency PSPs evoked by whisker deflection. *C*, *left traces*: average response to AW deflection for the cell in *A*. *Right graph*: plot of V_m vs. current injected for the AW-evoked response at 2 time points: baseline (filled circle) and during the PSP (open squares). Slope of the best-fit line through each set of points gives the apparent input resistance (R_{in}) of the cell at that time. *D*: average response ratios for the number and amplitude of whisker-evoked PSPs and the cumulative spike output for the population of intracellular recordings (black bars, $n = 15$). All values were significantly <1, indicating suppression. Average response ratios for PSP amplitude and R_{in} are also shown for a subset of cells (gray bars, $n = 4$).

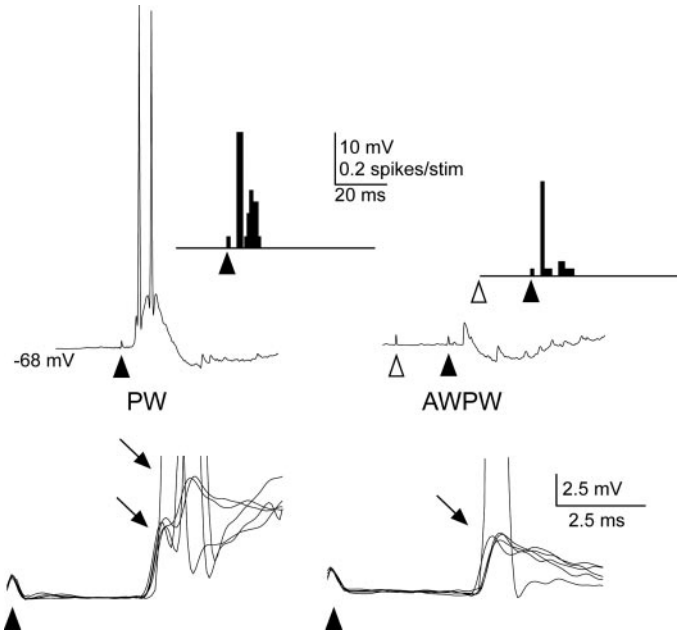

FIG. 8. Suppression of thalamic responses in the absence of AW-evoked synaptic excitation. Example traces and corresponding histograms illustrate synaptic and spike responses to PW deflection and paired AWPW deflection in a VPm cell. PW deflection evoked an initial burst of PSPs followed by a hyperpolarization from resting V_m (−68 mV). Preceding AW deflection did not evoke a synaptic excitatory response but resulted in suppression of both the number and amplitude of the PW-evoked synaptic response as well as spike output. Five overlaid traces in response to PW deflection alone (*left*) or paired AWPW deflection (*right*) are shown below.

the nearly 55% reduction in the cortical synaptic response both before and after cortical inactivation.

These data are the first demonstration of cross-whisker suppression in the trigeminal brain stem, although the results are consistent with previous work showing that both AW and PW deflection lead to suppression of spontaneous activity in PrV neurons (Minnery and Simons 2003). Our findings are further supported by both anatomical demonstrations of inhibitory circuitry within the trigeminal complex (Bae et al. 2000; Ginestal and Matute 1993) and physiological studies of PrV neurons in vitro showing synaptic excitation and feedforward inhibition evoked by afferent stimulation (Lo et al. 1999).

The synaptic responses in VPm neurons constituted bursts of unitary all-or-none PSPs, also observed in previous studies (Castro-Alamancos 2002a; Deschenes et al. 2003). This finding is consistent with extracellular recordings of whisker-evoked bursts in PrV neurons (Deschenes et al. 2003; our data, not shown) as well as with the intrinsic properties of trigeminal neurons that promote burst firing by persistent sodium currents (Enomoto et al. 2006). Suprathreshold responses consisting of single spikes were often evoked from resting V_m after the temporal summation of two to four PSPs. Spike output was truncated by a long-lasting inhibitory potential, presumably mediated by inputs from the thalamic reticular nucleus (nRT) (Pinault and Deschenes 1998; Varga et al. 2002), given that VPm is devoid of intrinsic inhibitory interneurons (Barbaresi et al. 1986). Both PW and AW deflection frequently evoked a similar pattern of excitation followed by inhibition, consistent with our extracellular data as well as with previous reports of multiwhisker receptive fields in VPm-projecting neurons in PrV (Minnery and Simons 2003; Timofeeva et al. 2004). Additionally, anatomical studies showed that fibers from nRT provide divergent feedback inhibition to VPm cells with receptive fields centered on neighboring PWs (Pinault and Deschenes 1998; Varga et al. 2002). Extracellular physiological studies also previously demonstrated strong inhibition of VPm spike output after either PW or AW deflection that was blocked by either pharmacological antagonism of GABA receptors or nRT lesion (Lee et al. 1994a,b). This inhibition is the likely explanation for the AW-mediated decrease in PW-evoked trigeminothalamic PSP amplitude, a conclusion supported by the similar values for the AW-mediated reduction in membrane R_{in} and the decreased PW-evoked PSP amplitude. Although trigeminothalamic synaptic depression was also observed (Castro-Alamancos 2002b), this mechanism is less likely to account for the decreased PSP amplitude because suppression was observed in cases where AW deflection did not result in an observable excitatory synaptic response.

To study cross-whisker suppression of cortical responses, we combined extracellular recordings of whisker-evoked LFPs with CSD analysis. As in previous studies (Di et al. 1990; Swadlow et al. 2002), PW deflection resulted in a spatial and temporal pattern of current sinks, thought to be a reflection of postsynaptic excitation (Mitzdorf 1985), that was consistent with known cortical anatomy. Thalamocortical fibers terminate primarily in cortical layers 4, deep 5, and 6 (Arnold et al. 2001; Jensen and Killackey 1987). Accordingly, PW deflection evoked the earliest current sinks (about 5 ms onset latency) in GR and IG layers, followed by a later sink in SG layers, in agreement with the well-characterized flow of excitation within a barrel column (Armstrong-James et al. 1992; Swadlow et al. 2002; Wirth and Luscher 2004). Cortical inactivation eliminated the PW-evoked SG current sink and reduced the magnitude and duration of sinks in GR and IG layers. However, the onset latencies in GR and IG layers were unchanged, suggesting that the remaining response was a direct reflection of thalamocortical synaptic input. The similar preservation of the AW-evoked cortical response after muscimol supports recent data indicating that multiwhisker cortical receptive fields are synthesized at subcortical levels (Kwegyir-Afful et al. 2005; Timofeeva et al. 2004).

We found a strong agreement between the magnitude of cross-whisker suppression for the cortical synaptic response measured with CSD analysis and the suppression of PW-evoked thalamic spike output (roughly 55%). It is important to note that the exact transformation of whisker-evoked thalamic activity into a cortical synaptic response and corresponding pattern of local current sinks and sources has not been explored in detail. However, this value of suppression is very similar to the magnitude of divisive PSP amplitude reduction seen in previous intracellular studies of cortical suppression (Higley and Contreras 2003, 2005), suggesting that the CSD analysis is a valid analogue to intracellular data. Importantly, there was no significant change in the magnitude of suppression after cortical inactivation. Although it is difficult to directly compare the cortical response before and after muscimol application, our results indicate that intracortical mechanisms that may influence normal sensory responses, including local postsynaptic inhibition (Connors et al. 1988; Kyriazi et al. 1996), presynaptic inhibition of thalamocortical terminals (Porter and Nieves 2004), and corticofugal feedback to earlier stages of sensory processing (Temereanca and Simons 2004), are not necessary

for the occurrence of cross-whisker suppression. In addition, the close agreement of the thalamic and cortical data suggests that thalamocortical synaptic depression, known to occur in the barrel system (Castro-Alamancos 2004; Chung et al. 2002), does not substantially contribute to suppression.

Previous extracellular studies observed stronger cross-whisker suppression of cortical versus thalamic spike output (Brumberg et al. 1996; Kyriazi et al. 1996; Simons and Carvell 1989). Moreover, Kyriazi et al. (1996) reported that blocking local cortical inhibition using bicuculline resulted in larger response ratios. These findings led to the hypothesis that intracortical mechanisms such as postsynaptic inhibition contribute to suppression. However, as with our present data from VPm, intracellular recordings previously showed that suppression of cortical spike output is significantly greater than the suppression of the underlying synaptic input as a result of the nonlinearity imposed by spike threshold (Higley and Contreras 2005, 2003). Furthermore, spike generation imposes an upper limit on the suprathreshold output of cortical neurons, contributing to a ceiling effect of response magnitude observed as stimulus intensity increases (Pinto et al. 2000; Wilent and Contreras 2004). Kyriazi et al. (1996) showed that the response to both PW and paired AWPW deflection increased after blocking inhibition. However, the initially larger PW-evoked response increased less, most likely explained by the ceiling effect, leading to a greater response ratio (AWPW/PW) despite potential preservation of the underlying suppression of synaptic inputs. In sum, these previous studies, in combination with the present data, are most consistent with the hypothesis that the underlying mechanism of suppression is subcortical. However, the process of spike generation may serve to further amplify spike suppression beyond the reduction in synaptic input.

Our finding that cortical inactivation did not alter the responsiveness of thalamocortical neurons in VPm is consistent with previous data (Fox et al. 2003), although Ghazanfar and Nicolelis (2001) found that cortical inactivation could result in either increases or decreases in thalamic responsiveness. Our results are somewhat surprising given the role of corticothalamic feedback in modulating whisker-evoked thalamic responses (Temereanca and Simons 2004). However, previous work suggested that the spontaneous firing rates of corticothalamic neurons are extremely low (Swadlow 1989), making it likely that the muscimol-induced reduction in cortical activity may have only a limited effect on this feedback circuit.

An additional intriguing finding from these data are that the engagement of local circuitry in cortical input layers appears to amplify the response to thalamic input under normal conditions. After muscimol application, the PW-evoked GR current sinks closely followed the rise time and decay of the thalamic population spike output. In contrast, the cortical response under control conditions was prolonged in duration relative to thalamic output. This observation supports previous hypotheses that corticocortical circuits play a role in amplifying afferent input, possibly through recurrent excitatory connections or intrinsic voltage-dependent *N*-methyl-D-aspartate conductances (Beierlein et al. 2002; Douglas et al. 1995; Fleidervish et al. 1998). Interestingly, the finding that cortical response suppression was proportionally the same in the presence or absence of recurrent activity suggests that the magnitude of cortical amplification may be a linear function of thalamic input.

Finally, the results presented here were obtained under light isoflurane anesthesia for a single interstimulus interval (20 ms) using high-velocity whisker deflections. Similar cross-whisker suppression of cortical responses at this interval was previously observed under barbiturate (Boloori and Stanley 2006; Higley and Contreras 2003), urethane (Shimegi et al. 1999), and fentanyl (Kyriazi et al. 1996) anesthesia (although, for less suppression under fentanyl see Simons and Carvell 1989). However, previous reports indicated that interactions at much shorter intervals (<5 ms) may involve facilitation rather than suppression (Ghazanfar and Nicolelis 1997; Higley and Contreras 2005; Shimegi et al. 1999). The role of subcortical circuits in mediating such facilitation remains to be determined. Furthermore, whisker-evoked cortical inhibition is known to be enhanced at higher stimulus velocities (Wilent and Contreras 2004) and intrathalamic inhibition may be similarly modulated. Future experiments are necessary to address this latter possibility and characterize the interaction of deflection kinematics and suppression.

In conclusion, our findings demonstrate that sensory suppression in the barrel system shows little dependency on local postsynaptic inhibition in the cortex. Instead, suppression occurs through a combination of reduced trigeminothalamic input, postsynaptic inhibition in VPm, and amplification by spike threshold mechanisms within the thalamus and cortex. These results present a clear example of a synergistic interaction between multiple stages of the afferent pathway. In the barrel system, similar multistage computations may enhance the sensitivity to deflection velocity (Deschenes et al. 2003; Pinto et al. 2000; Wilent and Contreras 2004) and sharpen directional tuning (Bruno and Simons 2002; Minnery and Simons 2003; Simons and Carvell 1989; Wilent and Contreras 2005). Sensory suppression has also been explored in other modalities, including the visual and auditory systems (Bair 2005; Schreiner et al. 2000). As with earlier literature in the whisker system, suppression of visual and auditory evoked responses has been attributed to local cortical inhibition (Bolz and Gilbert 1986; Cavanaugh et al. 2002; Hubel and Wiesel 1965; Mickey and Middlebrooks 2005; Ojima and Murakami 2002). However, recent reports in these areas also described suppression in subcortical structures (Fitzpatrick et al. 1999; Ozeki et al. 2004; Walker et al. 1999; Webb et al. 2005; Wehr and Zador 2005). These findings, coupled with the present results, suggest that functional synergism between multiple levels of afferent processing may be a general property of sensory systems.

ACKNOWLEDGMENTS

The authors thank Dr. Jessica A. Cardin for helpful discussion on this manuscript and Dr. Esther Garcia de Yebenes for help with histological preparation.

GRANTS

This work was supported by the Human Frontier Science Program.

REFERENCES

Armstrong-James M, Fox K, Das-Gupta A. Flow of excitation within rat barrel cortex on striking a single vibrissa. *J Neurophysiol* 68: 1345–1358, 1992.

Arnold PB, Li CX, Waters RS. Thalamocortical arbors extend beyond single cortical barrels: an in vivo intracellular tracing study in rat. *Exp Brain Res* 136: 152–168, 2001.

Bae YC, Ihn HJ, Park MJ, Ottersen OP, Moritani M, Yoshida A, Shigenaga Y. Identification of signal substances in synapses made between

primary afferents and their associated axon terminals in the rat trigeminal sensory nuclei. *J Comp Neurol* 418: 299–309, 2000.

Bair W. Visual receptive field organization. *Curr Opin Neurobiol* 15: 459–464, 2005.

Barbaresi P, Spreafico R, Frassoni C, Rustioni A. GABAergic neurons are present in the dorsal column nuclei but not in the ventroposterior complex of rats. *Brain Res* 382: 305–326, 1986.

Beierlein M, Fall CP, Rinzel J, Yuste R. Thalamocortical bursts trigger recurrent activity in neocortical networks: layer 4 as a frequency-dependent gate. *J Neurosci* 22: 9885–9894, 2002.

Boloori AR, Stanley GB. The dynamics of spatiotemporal response integration in the somatosensory cortex of the vibrissa system. *J Neurosci* 26: 3767–3782, 2006.

Bolz J, Gilbert CD. Generation of end-inhibition in the visual cortex via interlaminar connections. *Nature* 320: 362–365, 1986.

Brecht M, Preilowski B, Merzenich MM. Functional architecture of the mystacial vibrissae. *Behav Brain Res* 84: 81–97, 1997.

Brumberg JC, Pinto DJ, Simons DJ. Spatial gradients and inhibitory summation in the rat whisker barrel system. *J Neurophysiol* 76: 130–140, 1996.

Bruno RM, Simons DJ. Feedforward mechanisms of excitatory and inhibitory cortical receptive fields. *J Neurosci* 22: 10966–10975, 2002.

Carvell GE, Simons DJ. Biometric analyses of vibrissal tactile discrimination in the rat. *J Neurosci* 10: 2638–2648, 1990.

Castro-Alamancos MA. Different temporal processing of sensory inputs in the rat thalamus during quiescent and information processing states in vivo. *J Physiol* 539: 567–578, 2002a.

Castro-Alamancos MA. Properties of primary sensory (lemniscal) synapses in the ventrobasal thalamus and the relay of high-frequency sensory inputs. *J Neurophysiol* 87: 946–953, 2002b.

Castro-Alamancos MA. Absence of rapid sensory adaptation in neocortex during information processing states. *Neuron* 41: 455–464, 2004.

Cavanaugh JR, Bair W, Movshon JA. Nature and interaction of signals from the receptive field center and surround in macaque V1 neurons. *J Neurophysiol* 88: 2530–2546, 2002.

Chung S, Li X, Nelson SB. Short-term depression at thalamocortical synapses contributes to rapid adaptation of cortical sensory responses in vivo. *Neuron* 34: 437–446, 2002.

Connors BW, Malenka RC, Silva LR. Two inhibitory postsynaptic potentials, and GABAA and GABAB receptor-mediated responses in neocortex of rat and cat. *J Physiol* 406: 443–468, 1988.

Deschenes M, Timofeeva E, Lavallee P. The relay of high-frequency sensory signals in the whisker-to-barreloid pathway. *J Neurosci* 23: 6778–6787, 2003.

Di S, Baumgartner C, Barth DS. Laminar analysis of extracellular field potentials in rat vibrissa/barrel cortex. *J Neurophysiol* 63: 832–840, 1990.

Douglas RJ, Koch C, Mahowald M, Martin KA, Suarez HH. Recurrent excitation in neocortical circuits. *Science* 269: 981–985, 1995.

Enomoto A, Han JM, Hsiao CF, Wu N, Chandler SH. Participation of sodium currents in burst generation and control of membrane excitability in mesencephalic trigeminal neurons. *J Neurosci* 26: 3412–3422, 2006.

Fitzpatrick DC, Kuwada S, Kim DO, Parham K, Batra R. Responses of neurons to click-pairs as simulated echoes: auditory nerve to auditory cortex. *J Acoust Soc Am* 106: 3460–3472, 1999.

Fleidervish IA, Binshtok AM, Gutnick MJ. Functionally distinct NMDA receptors mediate horizontal connectivity within layer 4 of mouse barrel cortex. *Neuron* 21: 1055–1065, 1998.

Fox K, Wright N, Wallace H, Glazewski S. The origin of cortical surround receptive fields studied in the barrel cortex. *J Neurosci* 23: 8380–8391, 2003.

Freeman JA, Nicholson C. Experimental optimization of current source-density technique for anuran cerebellum. *J Neurophysiol* 38: 369–382, 1975.

Gardner EP, Costanzo RM. Temporal integration of multiple-point stimuli in primary somatosensory cortical receptive fields of alert monkeys. *J Neurophysiol* 43: 444–468, 1980.

Ghazanfar AA, Krupa DJ, Nicolelis MA. Role of cortical feedback in the receptive field structure and nonlinear response properties of somatosensory thalamic neurons. *Exp Brain Res* 141: 88–100, 2001.

Ghazanfar AA, Nicolelis MA. Nonlinear processing of tactile information in the thalamocortical loop. *J Neurophysiol* 78: 506–510, 1997.

Ginestal E, Matute C. Gamma-aminobutyric acid-immunoreactive neurons in the rat trigeminal nuclei. *Histochemistry* 99: 49–55, 1993.

Hartmann MJ, Johnson NJ, Towal RB, Assad C. Mechanical characteristics of rat vibrissae: resonant frequencies and damping in isolated whiskers and in the awake behaving animal. *J Neurosci* 23: 6510–6519, 2003.

Higley MJ, Contreras D. Nonlinear integration of sensory responses in the rat barrel cortex: an intracellular study in vivo. *J Neurosci* 23: 10190–10200, 2003.

Higley MJ, Contreras D. Integration of synaptic responses to neighboring whiskers in rat barrel cortex in vivo. *J Neurophysiol* 93: 1920–1934, 2005.

Hubel DH, Wiesel TN. Receptive fields and functional architecture in two nonstriate visual areas (18 and 19) of the cat. *J Neurophysiol* 28: 229–289, 1965.

Jensen KF, Killackey HP. Terminal arbors of axons projecting to the somatosensory cortex of the adult rat. I. The normal morphology of specific thalamocortical afferents. *J Neurosci* 7: 3529–3543, 1987.

Kida H, Shimegi S, Sato H. Similarity of direction tuning among responses to stimulation of different whiskers in neurons of rat barrel cortex. *J Neurophysiol* 94: 2004–2018, 2005.

Krupa DJ, Matell MS, Brisben AJ, Oliveira LM, Nicolelis MA. Behavioral properties of the trigeminal somatosensory system in rats performing whisker-dependent tactile discriminations. *J Neurosci* 21: 5752–5763, 2001.

Kwegyir-Afful EE, Bruno RM, Simons DJ, Keller A. The role of thalamic inputs in surround receptive fields of barrel neurons. *J Neurosci* 25: 5926–5934, 2005.

Kyriazi HT, Carvell GE, Brumberg JC, Simons DJ. Quantitative effects of GABA and bicuculline methiodide on receptive field properties of neurons in real and simulated whisker barrels. *J Neurophysiol* 75: 547–560, 1996.

Laaris N, Carlson GC, Keller A. Thalamic-evoked synaptic interactions in barrel cortex revealed by optical imaging. *J Neurosci* 20: 1529–1537, 2000.

Laskin SE, Spencer WA. Cutaneous masking. I. Psychophysical observations on interactions of multipoint stimuli in man. *J Neurophysiol* 42: 1048–1060, 1979a.

Laskin SE, Spencer WA. Cutaneous masking. II. Geometry of excitatory and inhibitory receptive fields of single units in somatosensory cortex of the cat. *J Neurophysiol* 42: 1061–1082, 1979b.

Lee SM, Friedberg MH, Ebner FF. The role of GABA-mediated inhibition in the rat ventral posterior medial thalamus. I. Assessment of receptive field changes following thalamic reticular nucleus lesions. *J Neurophysiol* 71: 1702–1715, 1994a.

Lee SM, Friedberg MH, Ebner FF. The role of GABA-mediated inhibition in the rat ventral posterior medial thalamus. II. Differential effects of $GABA_A$ and $GABA_B$ receptor antagonists on responses of VPM neurons. *J Neurophysiol* 71: 1716–1726, 1994b.

Llinás RR, Leznik E, Urbano FJ. Temporal binding via cortical coincidence detection of specific and nonspecific thalamocortical inputs: a voltage-dependent dye-imaging study in mouse brain slices. *Proc Natl Acad Sci USA* 99: 449–454, 2002.

Lo FS, Guido W, Erzurumlu RS. Electrophysiological properties and synaptic responses of cells in the trigeminal principal sensory nucleus of postnatal rats. *J Neurophysiol* 82: 2765–2775, 1999.

Mickey BJ, Middlebrooks JC. Sensitivity of auditory cortical neurons to the locations of leading and lagging sounds. *J Neurophysiol* 94: 979–989, 2005.

Minnery BS, Simons DJ. Response properties of whisker-associated trigeminothalamic neurons in rat nucleus principalis. *J Neurophysiol* 89: 40–56, 2003.

Mitzdorf U. Current source-density method and application in cat cerebral cortex: investigation of evoked potentials and EEG phenomena. *Physiol Rev* 65: 37–100, 1985.

Moore CI, Nelson SB, Sur M. Dynamics of neuronal processing in rat somatosensory cortex. *Trends Neurosci* 22: 513–520, 1999.

Mountcastle V. Neural mechanisms in somesthesia. In: *Medical Physiology*, edited by Mountcastle V. St. Louis, MO: Mosby, 1974.

Ojima H, Murakami K. Intracellular characterization of suppressive responses in supragranular pyramidal neurons of cat primary auditory cortex in vivo. *Cereb Cortex* 12: 1079–1091, 2002.

Ozeki H, Sadakane O, Akasaki T, Naito T, Shimegi S, Sato H. Relationship between excitation and inhibition underlying size tuning and contextual response modulation in the cat primary visual cortex. *J Neurosci* 24: 1428–1438, 2004.

Pinault D, Deschenes M. Anatomical evidence for a mechanism of lateral inhibition in the rat thalamus. *Eur J Neurosci* 10: 3462–3469, 1998.

Pinto DJ, Brumberg JC, Simons DJ. Circuit dynamics and coding strategies in rodent somatosensory cortex. *J Neurophysiol* 83: 1158–1166, 2000.

Porter JT, Nieves D. Presynaptic $GABA_B$ receptors modulate thalamic excitation of inhibitory and excitatory neurons in the mouse barrel cortex. *J Neurophysiol* 92: 2762–2770, 2004.

Sachdev RN, Sellien H, Ebner F. Temporal organization of multi-whisker contact in rats. *Somatosens Mot Res* 18: 91–100, 2001.

Schreiner CE, Read HL, Sutter ML. Modular organization of frequency integration in primary auditory cortex. *Annu Rev Neurosci* 23: 501–529, 2000.

Shimegi S, Ichikawa T, Akasaki T, Sato H. Temporal characteristics of response integration evoked by multiple whisker stimulations in the barrel cortex of rats. *J Neurosci* 19: 10164–10175, 1999.

Simons DJ, Carvell GE. Thalamocortical response transformation in the rat vibrissa/barrel system. *J Neurophysiol* 61: 311–330, 1989.

Swadlow HA. Efferent neurons and suspected interneurons in S-1 vibrissa cortex of the awake rabbit: receptive fields and axonal properties. *J Neurophysiol* 62: 288–308, 1989.

Swadlow HA, Gusev AG, Bezdudnaya T. Activation of a cortical column by a thalamocortical impulse. *J Neurosci* 22: 7766–7773, 2002.

Temereanca S, Simons DJ. Functional topography of corticothalamic feedback enhances thalamic spatial response tuning in the somatosensory whisker/barrel system. *Neuron* 41: 639–651, 2004.

Timofeeva E, Lavallee P, Arsenault D, Deschenes M. Synthesis of multi-whisker-receptive fields in subcortical stations of the vibrissa system. *J Neurophysiol* 91: 1510–1515, 2004.

Varga C, Sik A, Lavallee P, Deschenes M. Dendroarchitecture of relay cells in thalamic barreloids: a substrate for cross-whisker modulation. *J Neurosci* 22: 6186–6194, 2002.

Walker GA, Ohzawa I, Freeman RD. Asymmetric suppression outside the classical receptive field of the visual cortex. *J Neurosci* 19: 10536–10553, 1999.

Webb BS, Tinsley CJ, Vincent CJ, Derrington AM. Spatial distribution of suppressive signals outside the classical receptive field in lateral geniculate nucleus. *J Neurophysiol* 94: 1789–1797, 2005.

Wehr M, Zador AM. Synaptic mechanisms of forward suppression in rat auditory cortex. *Neuron* 47: 437–445, 2005.

Wilent WB, Contreras D. Synaptic responses to whisker deflections in rat barrel cortex as a function of cortical layer and stimulus intensity. *J Neurosci* 24: 3985–3998, 2004.

Wilent WB, Contreras D. Dynamics of excitation and inhibition underlying stimulus selectivity in rat somatosensory cortex. *Nat Neurosci* 8: 1364–1370, 2005.

Wirth C, Luscher HR. Spatiotemporal evolution of excitation and inhibition in the rat barrel cortex investigated with multielectrode arrays. *J Neurophysiol* 91: 1635–1647, 2004.